Simulating Multibody Dynamics With Rough Contact Surfaces and Run-in Wear

JANKO SLAVIČ* and MIHA BOLTEŽAR

*Faculty of Mechanical Engineering, Laboratory for Dynamics of Machines and Structures, University of Ljubljana, Askerceva 6, 1000 Ljubljana, Slovenia; *Author for correspondence (e-mail: janko.slavic@fs.uni-lj.si; fax: 386 125.18567)*

Abstract. The overall dynamics of a multibody system is actually a multi-scale problem because it depends a great deal on the local contact properties (coefficient of restitution, friction, roughness, etc). In this paper we found that the briefly presented force-based theory of plane dynamics for a multibody system with unilateral contacts was appropriate for simulating detailed multi-contact situations of rough contacting surfaces.

The focus of the paper is on a geometrically detailed description of rough surfaces. To achieve the run-in effect of the contacting surfaces under dynamical loads the contacting surfaces need to be re-shaped. For the re-shaping a wear model based on the local loss of mechanical energy under dynamical loads is presented.

The new ideas are presented for a numerical analysis of measuring the coefficient of friction at the rim of a wheel (rotating body). With the help of the analysis the experimentally observed change in the measured coefficient of friction of up to 30% for only slightly altered experimental conditions is explained.

Key words: brake dynamics, loss of mechanical energy at contacts, multibody dynamics, re-shaping, rough, unilateral contacts, wear model

1. Introduction

The mathematical formulation of multibody dynamics with unilateral contacts has received much interest in recent decades; however, it was only in the past decade that the formulation was developed to the necessary mathematical and physical consistency. Some of the first studies on multibody dynamics with bilateral contacts were done by Vereshchagin [29], Armstrong and Green [2] and Featherston [3] in the 1970s and 1980s.

The first studies of unilateral contacts in the form of a linear complementarity problem were published by Lötstedt [16, 17].

In recent years, the *time-stepping methods* which are due to Moreau [19] are being developed particularly rapidly. These methods operate in the impulse-velocity domain; therefore, at impact there is no need to switch from the force-acceleration domain to the impulse-velocity domain. Furthermore, these methods do not need to find the impact time, but usually use very small fixed time-step which defines the precision of the simulation. These methods are robust, easily to implement and can be used for dynamical systems with large number of contacts. An important contribution to the time-stepping methods was made by Monteiro-Marques [18], Paoli and Schatzman [21, 22], who studied the convergence of the solution, and also by Stewart and Trinkle [26, 27], Anitesca and Potra [1] and others.

In comparison to the time-stepping methods the event-driven methods use normal ODE integration methods at smooth contact-free phases and switch to contacts-solving at contact events. The accuracy of event-driven methods can be higher then the accuracy of time-stepping methods, but the event-driven methods are not appropriate for large number of contacts. Furthermore, the time-stepping as a numerical

method may overcome some difficulties (such as accumulation points) that can not be handled in a convincing way by e.g, the event-driven methods. A comparison of both methods is given in the work of Leine and Nijmeijer [14].

In this research Pfeiffer and Glocker [4, 23] event-driven formulation is used; their work presents a mathematically clear and physically consistent basis for plane contact dynamics and is superior to the classical approach in its uniform way of solving the stick-slip, detachment and impact events. There is also no need to adapt the number of generalized coordinates at any time. The strength of the formulation is in its simplicity and generality of use. Pfeiffer and Glocker introduced a new friction decomposition that avoids singularities in the presence of dependent coordinates and can also handle over-constrained systems. They also introduced, for the first time, the impact law with friction as a linear complementary problem [23].

The friction decomposition presented in [4, 23] is quite cumbersome because it uses four unilateral primitives for one friction curve; however, a more advance decomposition which uses only two unilateral primitives was presented by Rossmann et al. [24] and extended to spatial friction as a nonlinear complementarity problem [5, 7]. Further extensions towards spatial systems can be found in [6, 10, 12].

The contact dynamics research is often focused towards simplified contacting surfaces of one contacting point only (e.g., the pad of a brake is reduced to a point mass [9]). However, the geometrically quite simple contacting surfaces are usually enhanced with advanced contact laws [8, 15, 31]. To research the importance of the geometrically detailed contacting surfaces in this research the force-based theory is used with basic contact laws but with geometrically complex contacting surfaces.

This work is organized as follows: in the second section of this research the formulation [4, 23] of multibody plane dynamics with unilateral contacts is adapted to bodies with arbitrary body shapes. The third section presents the local loss of mechanical energy and its role in defining the wear of contacting rough surfaces under dynamic loads. The fourth section presents a numerical example with run-in wear. In addition, an explanation for the apparent change of the coefficient of friction for disk-shaped bodies is given. The last section presents the conclusions.

2. Multibody Dynamics with Unilateral Contacts as a Linear Complementarity Problem

For the sake of completeness this section gives a brief review of the mathematical modeling of multibody dynamics with unilateral contacts as presented by Glocker and Pfeiffer [4, 23]. The methods are presented for linear contacts (plain dynamics), but with some modifications they can also be used for plane contacts (3D spatial dynamics) [5–7, 10, 12, 30].

The equations of motion for a multibody system with f degrees of freedom (including only bilateral contacts) can be written as:

$$\boldsymbol{M}(\boldsymbol{q}, t)\,\ddot{\boldsymbol{q}} - \boldsymbol{h}(\boldsymbol{q}, \dot{\boldsymbol{q}}, t) = \boldsymbol{0} \in \mathbb{R}^f, \tag{1}$$

where $\boldsymbol{M}$ is the mass matrix, $\boldsymbol{q}$ is the vector of generalized coordinates and $\boldsymbol{h}$ is the vector of generalized active forces. If there is a set of $i \in I_\mathrm{N}$ contact forces then the equations of motion will be:

$$\boldsymbol{M}\,\ddot{\boldsymbol{q}} - \boldsymbol{h} = \sum_{i \in I_\mathrm{N}} \boldsymbol{Q}_i^\mathrm{C} \in \mathbb{R}^f, \tag{2}$$

where $\boldsymbol{Q}_i^\mathrm{C}$ are the generalized, non-conservative active forces.
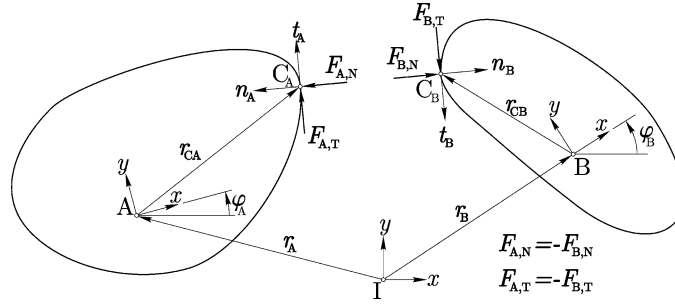
Figure 1. Contact forces.

Note that the contacts forces change the number of degrees of freedom. A priory it is not known which degrees of freedom disappear; this problem is usually solved by looking at all the possible solutions and finding the one that is physically consistent. If there are n_N possible contact points with a stick-slip transition or detachment, then there are 3^{n_N} possible solutions [23]. It is clear that the search for a physically consistent combination is time-consuming. Furthermore, for numerical simulations it is quite unsuitable to change the minimum number of coordinates during each time-step.

The event-driven integration method, using a LCP formulation to solve the contact problem solves this problem in an elegant way, and the number of generalized coordinates is constant at all times and equal to the number of degrees of freedom of the system without unilateral contacts (2).

The real contact forces are linked with the generalized contact forces via the Jacobian matrix. In Figure 1 two bodies are shown, the centres of gravity being denoted by A and B. The normal contact force $\boldsymbol{F}_{A,N}$ at point C_A on the body A as a generalized contact force is:

$$Q_{A,N}^{C} = \left(\frac{\partial\,_I\boldsymbol{r}_{C_A}}{\partial\,\boldsymbol{q}} \right)^{T} \boldsymbol{F}_{A,N} = \boldsymbol{J}_{C_A}^{T} \cdot\,_I\boldsymbol{n}_A \cdot \lambda_N, \tag{3}$$

where $\boldsymbol{J}_{C_A}^{T}$ is the Jacobian matrix of $_I\boldsymbol{r}_{C_A}$. $\boldsymbol{J}_{C_A}^{T}$ can be written as:

$$\boldsymbol{J}_{C_A} = \boldsymbol{J}_A + \boldsymbol{J}_{RA}, \tag{4}$$

where $\boldsymbol{J}_A$ is defined by $\boldsymbol{r}_A$ and $\boldsymbol{J}_{RA}$ by the relative vector $\boldsymbol{r}_{C_A}$ and the angle φ_A [25]. Furthermore, by using the Jacobian matrix, the relative contact acceleration $_I\ddot{\boldsymbol{r}}_{C_A} = \,_I\ddot{\boldsymbol{r}}_A + \,_I\ddot{\boldsymbol{r}}_{CA}$ is:

$$_I\ddot{\boldsymbol{r}}_{C_A} = \boldsymbol{J}_{C_A}\,\ddot{\boldsymbol{q}} + \bar{\boldsymbol{j}}_{C_A}, \tag{5}$$

where $\bar{\boldsymbol{j}}_{C_A}$ is the vector of missing velocity and position dependent values and is defined as:

$$\bar{\boldsymbol{j}}_{C_A} = \bar{\boldsymbol{j}}_A + \bar{\boldsymbol{j}}_{RA}. \tag{6}$$

where $\bar{\boldsymbol{j}}_A$ is defined by $\boldsymbol{r}_A$ and $\bar{\boldsymbol{j}}_{RA}$ by the relative vector $\boldsymbol{r}_{C_A}$ and the angle φ_A [25].

Further, by including the normal force at point B $\boldsymbol{Q}_N^C$ becomes:

$$\boldsymbol{Q}_N^C = \left(\boldsymbol{J}_{C_A}^{T}\,_I\boldsymbol{n}_A + \boldsymbol{J}_{C_B}^{T}\,_I\boldsymbol{n}_B \right) \lambda_N = \boldsymbol{w}_N\,\lambda_N. \tag{7}$$

$\boldsymbol{w}_N$ includes the kinematical properties of the contact, λ_N is the amplitude of the force and I denotes the inertial frame.

By using a similar notation for the tangential force (index T), Equation (2) is rewritten as:

$$M\,\ddot{q} - h - \sum_{i \in I_N}(w_N\,\lambda_N + w_T\,\lambda_T)_i = 0 \in \mathbb{R}^f. \tag{8}$$

Or by using matrix notation:

$$W_N = \{w_{Ni}\}, \quad W_T = \{w_{Ti}\}, \quad i \in I_N, \tag{9}$$

the equations of motion are:

$$M\,\ddot{q} - h - (W_N\ W_T)\begin{pmatrix}\lambda_N \\ \lambda_T\end{pmatrix} = 0 \in \mathbb{R}^f. \tag{10}$$

The contact situations are solved in two steps: in the first, the non-smooth impact with friction is solved (see Section 2.2); in the second the stick-slip or detachment situation is solved (see Section 2.1). While the impact is solved in the impulse-domain, the stick-slip or detachment is solved in the force-domain.

All the possible contact points I_G are organized in four sets during each time-step :

$$
\begin{aligned}
I_G &= \{1, 2, \ldots, n_G\} \\
I_S &= \{i \in I_G\,;\, g_N = 0\}\ n_S \text{ elements,} \\
I_N &= \{i \in I_S\,;\, \dot{g}_N = 0\}\ n_N \text{ elements,} \\
I_H &= \{i \in I_N\,;\, \dot{g}_T = 0\}\ n_H \text{ elements.}
\end{aligned}
\tag{11}
$$

The set I_S contains all the closed contacts, the set I_N contains only the contacts with vanishing relative normal velocities (stick-slip or detachment), and the set I_H contains the possibly sticking contacts. The number of elements in the sets can change during each time-step.

2.1. STICK-SLIP TRANSITION OR DETACHMENT

First, the stick-slip transition or detachment problem is solved on an impact-free set I_N. The equations of motion (10) and the relative contact accelerations $\ddot{g}$ are [4, 23, 13]:

$$M\,\ddot{q} - h - (W_N + W_G\,\bar{\mu}_G\,W_H)\begin{pmatrix}\lambda_N \\ \lambda_H\end{pmatrix} = 0 \in \mathbb{R}^f, \tag{12}$$

$$\begin{pmatrix}\ddot{g}_N \\ \ddot{g}_H\end{pmatrix} = \begin{pmatrix}W_N^T \\ W_H^T\end{pmatrix}\ddot{q} + \begin{pmatrix}\bar{w}_N \\ \bar{w}_H\end{pmatrix} \in \mathbb{R}^{n_N + n_H}. \tag{13}$$

The index N denotes the normal direction, and the index H denotes the tangential direction of the possibly sticking set I_H. The new index G denotes the sliding contacts (the tangential force is known) of the set $I_N \setminus I_H$ and the $\bar{\mu}_G$ diagonal matrix of friction coefficients. The additional $n_N + n_H$ equations that are needed to solve the Equations (12) and (13) are represented by the complementarity conditions in the normal and tangential directions, details are given in [23].

2.2. IMPACT WITH FRICTION

While the stick-slip or detachment transition is solved in the force-acceleration domain, the impact is solved in the impulse-velocity domain. Some common assumptions for rigid-body impacts are made: the duration of the impact is infinitely short, the wave effects are not taken into account, during the impact all positions and orientations, and all the non-impulsive forces and torques remain constant. The impact is divided into two phases: the compression phase (time interval: $t_A - t_C$) and the expansion phase (time interval: $t_C - t_E$). In this work Poisson's impact law is used.

For impacts the contacts of the set I_S are taken into account.

2.2.1. *Compression Phase*

The index C is used for the compression phase. By integrating the equation of motion (10) an impulse-domain equation is built [23]:

$$\boldsymbol{M}(\dot{\boldsymbol{q}}_C - \dot{\boldsymbol{q}}_A) - (\boldsymbol{W}_N \ \boldsymbol{W}_T) \begin{pmatrix} \boldsymbol{\Lambda}_{NC} \\ \boldsymbol{\Lambda}_{TC} \end{pmatrix} = \boldsymbol{0} \in \mathbb{R}^f. \tag{14}$$

The relative contact velocities are:

$$\begin{pmatrix} \dot{\boldsymbol{g}}_{NC} \\ \dot{\boldsymbol{g}}_{TC} \end{pmatrix} = \begin{pmatrix} \boldsymbol{W}_N^T \\ \boldsymbol{W}_T^T \end{pmatrix} (\dot{\boldsymbol{q}}_C - \dot{\boldsymbol{q}}_A) + \begin{pmatrix} \dot{\boldsymbol{g}}_{NA} \\ \dot{\boldsymbol{g}}_{TA} \end{pmatrix} \in \mathbb{R}^{2n_S}. \tag{15}$$

$\boldsymbol{\Lambda}_{NC}$ and $\boldsymbol{\Lambda}_{TC}$ are the contact impulses during the compression phase, and A and C represent the beginning and the end of the compression. Similarly, as before, for the missing $2n_s$ equations complementarity conditions in the normal and tangential directions can be found, details are given in [23].

2.2.2. *Expansion Phase*

The expansion phase starts from the end of the compression phase and is resolved in a similar way to the compression, except that some attention needs to be paid to the impenetrability conditions and, optionally, to the reversibility of the tangential contact [23].

3. Wear Model Under Dynamic Loads

When two (or more) bodies are in unilateral contact (sticking, slipping, impacting) then the contacting surfaces are exposed to mechanical wear. In order to identify the rate of mechanical wear in this research we used the loss of mechanical energy $W(s)$ at the contacting surfaces, see Figure 2.
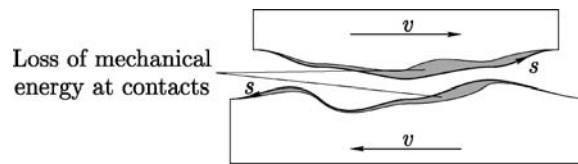

Figure 2. Two bodies in dynamical contact and the loss of mechanical energy (shaded).

The wear rate r_W is defined in terms of the maximum loss of mechanical energy of each body:

$$r_W(s) = \frac{W(s)}{\text{Max}(W)}.\tag{16}$$

The actual wear (reshaping) amplitude $u(s)$ of the contacting surfaces is:

$$u(s) = u_{\text{Max}}\, r_W(s),\tag{17}$$

where u_{Max} is the maximum change of shape (a measure of the size of the wear particle) between two simulations. The direction of reshaping is to the inside of the body, according to the normal contact vector, see Figure 1.

To achieve the steady-state contact-surface-shape usually several re-shapings need to be done. After each re-shaping the simulation needs to be run again to determine the loss of mechanical energy $W(s)$ at the current contact shapes.

3.1. Loss of Mechanical Energy in the Contact Situation

The loss of mechanical energy during impact situations (for stick-slip the procedures are very similar) is defined by the loss during the compression phase summed with the loss during the expansion phase.

During the compression phase the local loss of mechanical energy is defined as (A denotes the start of compression and C the end of compression):

$$W_{\text{C}} = \dot{\bar{\boldsymbol{g}}}_{\text{AC}}\, \boldsymbol{I}_{\text{C}},\tag{18}$$

where:

$$\boldsymbol{I}_{\text{C}} = {}_{\text{I}}\boldsymbol{n}\, \Lambda_{\text{NC}} + {}_{\text{I}}\boldsymbol{t}\, \Lambda_{\text{TC}}\tag{19}$$

is the impulse during the compression phase (in the local contact coordinate system) and:

$$\dot{\bar{\boldsymbol{g}}}_{\text{AC}} = \frac{\dot{\boldsymbol{g}}_{\text{A}} + \dot{\boldsymbol{g}}_{\text{C}}}{2}.\tag{20}$$

is the average relative contact velocity.

The loss of mechanical energy during the expansion phase is similar, except that the indexes are as follows: C is replaced with E, to denote the end of compression; and A is replaced with C, to denote the start of expansion.

4. Numerical Examples

4.1. Mathematical Model

In this section the presented methods will be shown on a numerical example of a sliding pin in contact with a round (rotating) surface, see Figure 3. The system has 2 degrees of freedom: the translational degree of freedom r and the rotational degree of freedom φ. As shown in Figure 3 in each of these directions a spring-damper element is present. The symbols s and v define the starting positions of the pin.
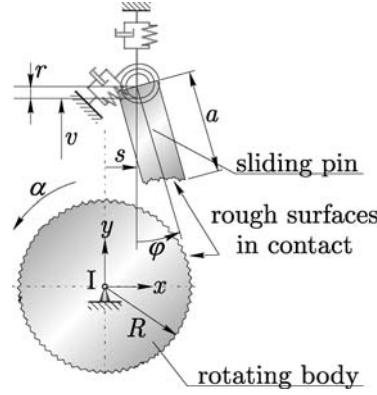
Figure 3. Mathematical model.

For a similar system Leine et al. [11] proved that the model can have non-uniqueness and even non-existence of solutions for arbitrary small critical friction coefficient which depends on the mass ratios of the system. Despite the fact that the system presented here differs from [11] we can estimate that the critical friction coefficient is well above 0.125 which was used in this study.

The set of generalized coordinates:

$$q = \begin{pmatrix} r \\ \varphi \end{pmatrix}. \tag{21}$$

The set of dependent coordinates:

$$d = \begin{pmatrix} x_p \\ y_p \\ \alpha \end{pmatrix} = \begin{pmatrix} s + \frac{1}{2} a \sin \varphi \\ v - \frac{1}{2} a \cos \varphi + r \\ 2 \pi f t \end{pmatrix}, \tag{22}$$

where x_p and y_p are the absolute coordinates of the pin's centre of gravity, a is the length of the pin and f is the rotating frequency in Hz. For the dependent coordinates the associated Jacobian vectors (used to build the Jacobian matrix (4)) are:

$$J_{x_p} = \frac{\partial x_p}{\partial q} = \left(0 \ \frac{1}{2} a \cos \varphi \right), \tag{23}$$

$$J_{y_p} = \frac{\partial y_p}{\partial q} = \left(1 \ \frac{1}{2} a \sin \varphi \right), \tag{24}$$

$$J_\alpha = \frac{\partial \alpha}{\partial q} = (0 \, 0) \tag{25}$$

And the associated coordinates that are used to build up the vector $\bar{j}$ (6):

$$\bar{j}_{x_p} = -\frac{1}{2} a \dot{\varphi}^2 \sin \varphi \tag{26}$$

$$\bar{j}_{y_p} = \frac{1}{2} a \dot{\varphi}^2 \cos \varphi \tag{27}$$

$$\bar{j}_\alpha = 0. \tag{28}$$

The mass matrix $\boldsymbol{M}$ and the vector of active forces $\boldsymbol{h}$:

$$\boldsymbol{M} = \begin{pmatrix} m & \frac{1}{2} a\, m\, \sin\varphi \\ \frac{1}{2} a\, m\, \sin\varphi & \frac{1}{4} a^2\, m\, \cos^2\varphi + \frac{1}{4} a^2\, m\, \sin^2\varphi + J_{zz} \end{pmatrix}, \tag{29}$$

$$\boldsymbol{h} = \begin{pmatrix} -\frac{1}{2} a\, m\, \cos\varphi\, \dot{\varphi}^2 - p\, k_\varphi - k_r\, r - c_r\, \dot{r} \\ -k_\varphi\, \varphi - c_\varphi\, \dot{\varphi} \end{pmatrix}. \tag{30}$$

Where a, m and J_{zz} are the length, mass and the mass moment of inertia (about the centre of gravity) of the pin, respectively. Furthermore, k_r, d_r and k_φ, d_φ are the stiffness and the damping parameters for the r and φ directions, respectively.

Finally, p is the parameter that defines the pre-stress in the spring in the r direction at $r = 0$. In the presented example the following parameters were used:

$a = 0.001$ m, $s = 0$ m, $v = 0.01200116$ m, $c_\varphi = 2.12\ 10^{-5}$ Nms/rad, $c_r = 4.32\ 10^{-2}$ Ns/m, $p = 9.40\ 10^{-6}$ m, $f = 4$ Hz, $k_\varphi = 0.0791$ Nm/rad, $k_r = 329.9$ kN/m.

Additionally, the width and the depth of the pin are equal to a, and the radius of the rotating body is $R = 0.011$ m, see Figure 3. The density of the pin is $\rho = 1650$ kg/m^3. The mass parameters are calculated according to the current shapes, which are about to change.

The used contact parameters are as follows $\mu = 0.125$, $\epsilon_N = 0.5$, $\epsilon_T = 0.5$, $v = 0$, where μ is the coefficient of friction and ϵ_N and ϵ_T are the coefficients of restitution in the normal and tangential directions. v is used for the reversibility in the tangential direction [23].

Simulation parameters. Usually, the largest natural frequency defines ($f_{r,0} = 210$ kHz and $f_{\varphi,0} = 103$ kHz) the time-step of the simulation; however, it was observed that the non-smooth impact situations are more critical and the longest time-step used in this simulation is therefore $T = 10^{-9}$ s.

The total time of the simulation, 10^{-3} s, corresponds to a relative displacement between the pin and the rotating body of 0.27 mm. The maximum allowed penetration depth between the bodies is $2.5 \cdot 10^{-8}$ m.

The roughness of the contacting surfaces. The roughness is added to the curvature of the contacting surfaces (i.e., the discrete points are randomized in the radial direction). The randomization should be in accordance with [20, 28], which have found that the average change of slope between two consecutive points is, on average, 10–15°. In this research the maximum change of slope was limited to 15°.

The simulated roughness of the pin is $Rz = 1.25\ \mu$m, and that of the rotating body is $Rz = 2.5\ \mu$m. The arch of the pin is described by 100 discrete points, which corresponds approximately to the distance between two points: $10\ \mu$m. A similar division between the discrete points is used for the rotating body. The roughness of these two bodies is shown in Figure 4.
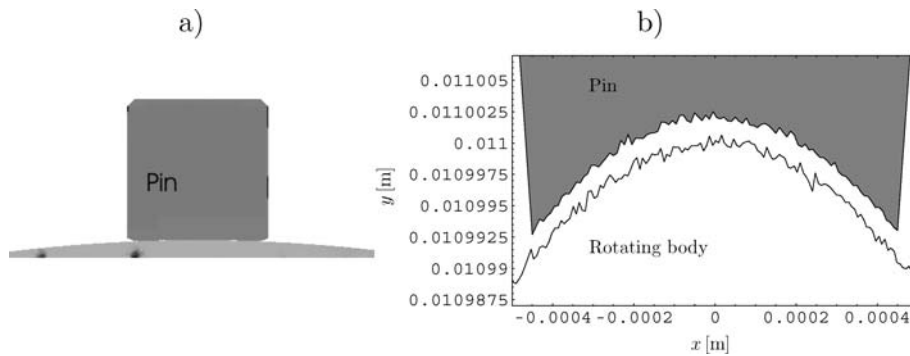

Figure 4. (a) Pin and the rotating body. (b) Detail of contacting asperities (moved apart). Scale ratio: $x/y = 1/50$.

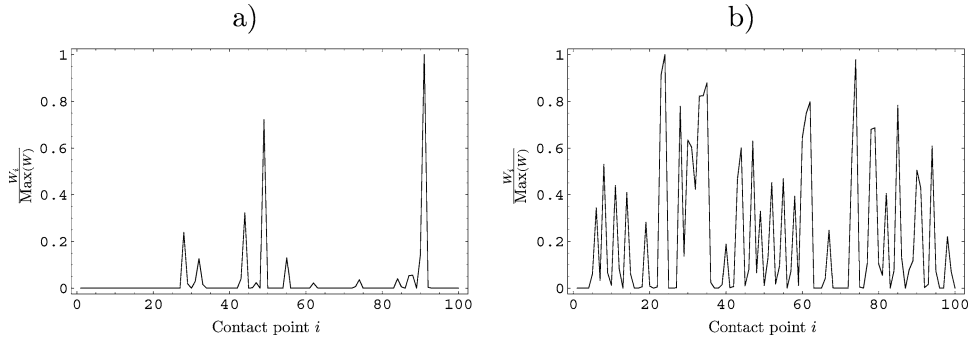a)   b)

Figure 5. Loss of mechanical energy: (a) at the initially rough contact surfaces, (b) at rough contact surfaces after five mechanical-energy-loss-based re-shaping steps.
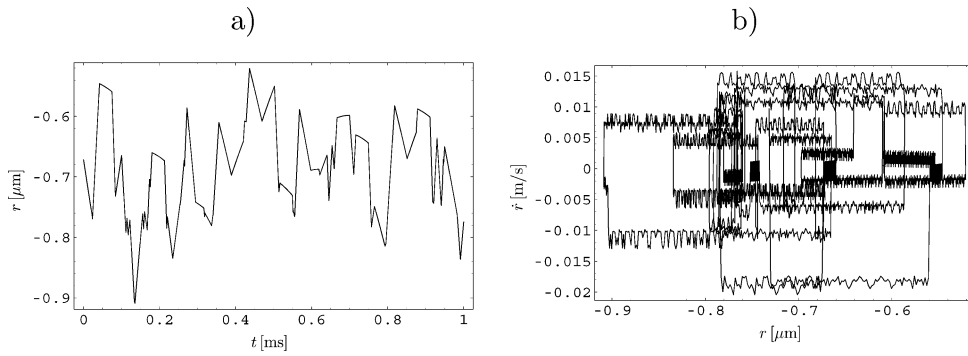
a)   b)

Figure 6. (a) time history of r, (b) phase plot of r.

4.2. RUN-IN PERIOD (WEAR)

During the run-in period the outstanding peaks of the initial roughness are quickly worn away.

In Figure 5a the loss of mechanical energy at the contact points of the initial roughness is shown; it is obvious that only a few contact points take all of the load.

In the next simulation step the contact surface of the initial simulation is re-shaped according to the wear-rate function r_W (16). The maximum used change of body shape is $u_{\text{Max}} = 0.15\,\mu$m.

The reshaping is not expected to alter the overall roughness properties significantly. After five re-shaping steps the loss of mechanical energy at the contact surface is more uniform, see Figure 5b.

The time histories and phase plots of r and φ after five re-shaping steps are shown in Figures 6 and 7, respectively. The effect of roughness can be clearly identified.

4.3. INFLUENCES ON THE MEASURED COORDINATE SYSTEM

By experimental means we have observed a strong influence of the parameter s in Figure 3 on the measured COF $\mu_{xy} = F_x/F_y$, where the measured coordinate system corresponds to the inertial one (xy), see Figure 3. We observed a change of $s = \pm 0.4$ mm to alter the measured COF up to 30%.

At first it seemed very strange that a change of only 0.4 mm for a radius of rotation of 11 mm changed the COF by up to 30%. One possibility was that the contact dynamics had changed (e.g., continuous sliding to stick-slip or vice versa).
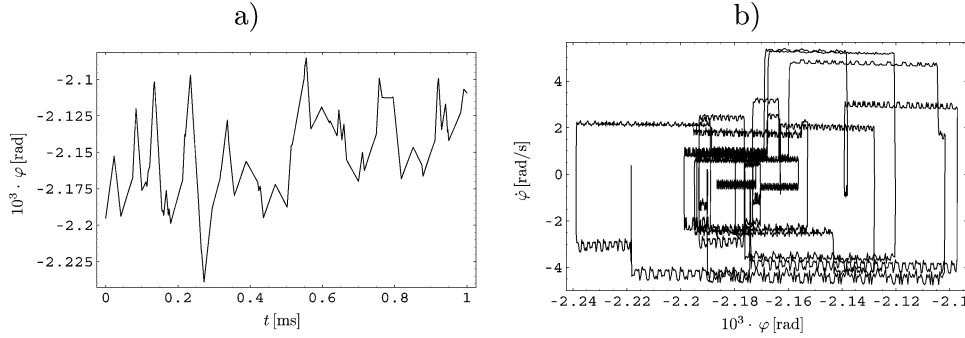
a)   b)

Figure 7. (a) time history of φ, (b) phase plot of φ.

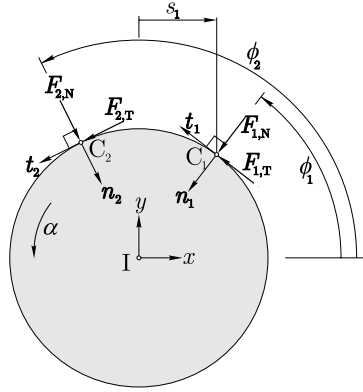*Figure 8.* Contact coordinate system (nt) and the measured coordinate system (xy). Note: $\cos\phi = s/R$.

An explanation for this change of the measured COF is given in the following.

Simple smooth contact model. We found a simple geometrical explanation by using a simple, one-contact-point model as appropriate, see Figure 8.

In the simple model the contact forces (the coordinate system nt) are measured as:

$$F_x = F_N \cos\phi + F_T \sin\phi \qquad F_y = F_N \sin\phi - F_T \cos\phi. \tag{31}$$

From the measured contact forces the coefficient of friction is defined as:

$$\mu_{xy,G} = \frac{F_x}{F_y} = \cot(\phi - \phi_\mu), \tag{32}$$

where the frictional force is defined by $F_T = F_N\,\mu = F_N \tan\phi_\mu$. It follows that for a constant friction parameter μ (or ϕ_μ) the measured COF will change according to the angle ϕ.

The measured COF $\mu_{xy,G}$ as a function of the translation parameter s would, using this simple model, be measured as shown in Figure 8.

The advanced rough-contact model. In the advanced model the parameter s denotes the position of the centre of mass of the pin. The concurred contact situations are much more complicated, and at each contact situation the angle ϕ depends on the local roughness of the rough surfaces in contact.
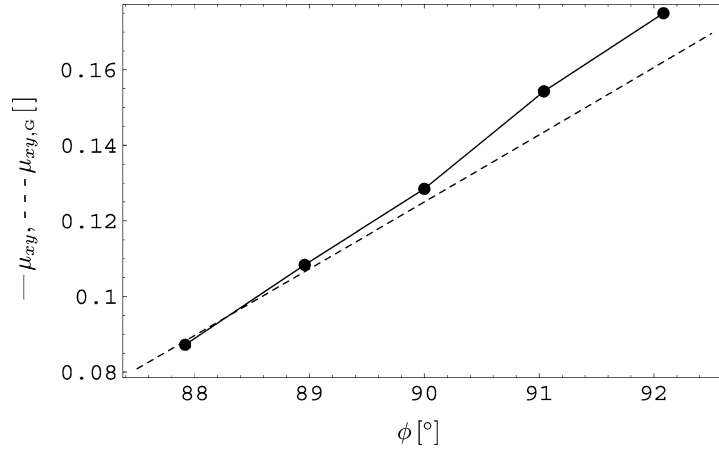
Figure 9. Comparison of the measured COF: - - - $\mu_{xy,\text{G}}$ simple model and —— μ_{xy} advanced model. The actual COF is $\mu = 0.125$.
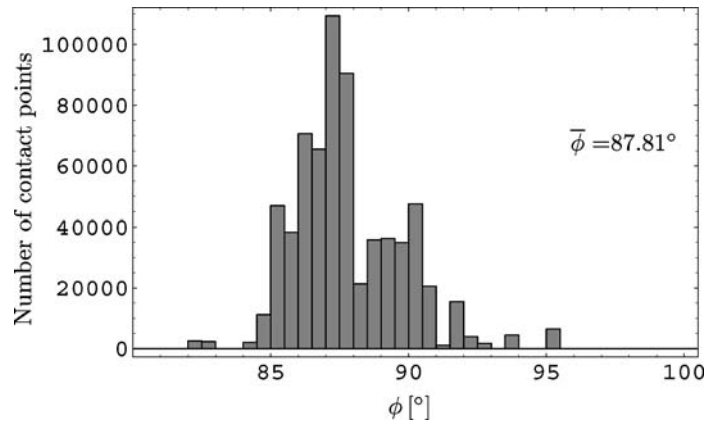

Figure 10. Histogram of contact angles of the advanced model at $s = +0.4\,\text{mm}$.

By comparing the COF of the advanced contact model μ_{xy} with the simple model $\mu_{xy,\text{G}}$ the conclusions are comparable, see Figure 9.

A detailed analysis would reveal that during the simulation approximately 700 thousand contact situations between the pin and the rotating body occurred. The histogram of the contact angles of the simulation with the pin at $s = +0.4\,\text{mm}$ (Figure 10) reveals that the contact angles are nearly normally distributed and the average contact angle of all the contact situations $\bar{\phi} = 87.81\,^\circ$. Despite the fact that the COF ($\mu = 0.125$) is constant the measured COF μ_{xy} decreases because of the average angle $\bar{\phi}$.

A detailed analysis of the advanced model revealed only continuous sliding and no stick-slip vibrations.

5. Conclusions

The theory of multibody dynamics with unilateral contacts is used to simulate the detailed contacts of rough surfaces. In reality, the outstanding asperities that take the majority of the dynamical load are

quickly worn away and the mechanical load is transferred to other contact points. The wear model based on the local loss of mechanical energy, as presented in this article, was found to be appropriate for the wear of the outstanding asperities. After the run-in period the dynamical load of the contacting rough surfaces is relatively uniform.

In the numerical example the experimentally observed decrease of the COF is studied. It was found that the reason for the change in the measured COF is not in the change of the contact dynamics, but because of the small difference between the measured coordinate system and the local contact coordinate system.

The numerical simulation showed that only with a perfectly centered friction tip a correct COF can be measured. A slightly misaligned measuring tip can result in large measurement errors; e.g., for a $2°$ misalignment an error of approximately 30% would be expected.

As shown in the numerical example the presented methods are expected to open new opportunities for analyzing the influence of detailed contact geometry on the dynamics of mechanical systems (e.g., brake-friction dynamics).

References

1. Anitescu, M. and Potra, F., 'Formulating dynamic multi-rigidbody contact problems with friction as solvable linear complementarity problems', *Nonlinear Dynamics* **14**, 1997, 231–247.
2. Armstrong, W. and Green, M., 'The dynamics of articulated rigid bodies for purposes of animation', *The Visual Computer* **1**, 1985, 231–240.
3. Featherstone, R., *Robot Dynamics Algorithms*, Kluwer, Dordrecht, 1987.
4. Glocker, C., 'Dynamik von Starrkörpersystemen mit Reibung und Stößen', Ph.D. thesis, Technische Universität München, 1995.
5. Glocker, C., 'Formulation of spatial contact situations in rigid multibody systems', *Computer Methods and Applications Mechenical Engineering* **177**, 1999, 199–214.
6. Glocker, C., *Set-Valued Force Laws: Dynamics of Non-Smooth Systems*, Lecture Notes in Applied Mechanics 1, Springer Verlag, Berlin, 2001.
7. Glocker, C. and Studer, C., 'Formulation and preparation for numerical evaluation of linear complementarity systems in dynamics', *Multibody System Dynamics* **13**, 2005, 447–463.
8. Harsha, S. P., Sandeep, K., and Prakash, R.,'Nonlinear dynamic response of a rotor bearing system due to surface waviness', *Nonlinear Dynamics* **37**(2), 2004, 91–114.
9. Heilig, J. and Wauer, J., 'Stability of a nonlinear brake system at high operating speeds', *Nonlinear Dynamics* **34**(3–4), 2003, 235–247.
10. Le Saux, C., Leine, R. I., and Glocker, C., 'Dynamics of a rolling disk in the presence of dry friction', *Journal of Nonlinear Science* **15**(1), 2005, 27–61.
11. Leine, R. I., Brogliato, B., and Nijmeijer, H., 'Periodic motion and bifurcations induced by the Painlevé paradox', *European Journal of Mechanics A/Solids* **21**, 2002, 869–896.
12. Leine, R. I. and Glocker, C., 'A set-valued force law for spatial Coulomb-Contensou friction', *European Journal of Mechanics A / Solids* **22**, 2003, 193–216.
13. Leine, R. I., Glocker, C., and Van Campen, D., 'Nonlinear dynamics and modelling of some wooden toys with impact and friction', *Nonlinear Dynamics* **9**, 2003, 25–78.
14. Leine, R. I. and Nijmeijer, H., *Dynamics and Bifurcations of Non-Smooth Mechanical Systems*, Vol. 18 of *Lecture Notes in Applied and Computational Mechanics*, Springer, New York, 2004.
15. Leine, R. I., Van Campen, D. H., Kraker, A., and Van den Steen, L., 'Stick-slip vibrations induced by alternate friction models', *Nonlinear Dynamics* **16**(1), 1998, 41–54.
16. Lötstedt, P., 'Coulomb friction in two-dimensional rigid body systems', *Zeifschrift für Angewandte Mathematik and Mechanik* **61**, 1981, 605–615.
17. Lötstedt, P., 'Mechanical systems of rigid bodies subject to unilateral constraints', *SIAM Journal of Applied Mathematics* **42**(2), 1982, 281–296.
18. Monteiro-Marques, M., *Differential Inclusions in Nonsmooth Mechanical Problems: Shocks and Dry Friction*, Vol. 9. Birkhäuser Verlag, Basel, Boston, Berlin, 1993.

19. Moreau, J.-J., *Unilateral Contact and Dry Friction in Finite Freedom Dynamics*, Nonsmooth Mechanics and Applications. Springer-Verlag, Vienna, New York. International Centre for Mechanical Sciences, Courses and Lectures 302, 1988, pp. 1–82.
20. Oden, J. and Martins, J., 'Models and computational methods for dynamic friction phenomena', *Computer Methods In Applied Mechanics And Engineering* **52**(1–3), 1985, 527–634.
21. Paoli, L. and Schatzman, M., 'Mouvement à un nombre fini de degrés de liberté avec contraintes unilatérales: Cas avec perte d'énergie', *Mathematical Modeling and Numerical Analysis* **27**, 1993a, 673ñ–717.
22. Paoli, L. and Schatzman, M., 'Vibrations avec contraintes unilatérales et perte d'énergie aux impacts, en dimension finie', *Comptes Rendus de l'Académie des Sciences Paris Sér. I* **317**, 1993b, 97ñ–101.
23. Pfeiffer, F. and Glocker, C., *Multibody Dynamics with Unilateral Contacts*, John Wiley & Sons, Inc, New York, 1996.
24. Rossmann, T. and Glocker, C., 'Efficient algorithms for non-smooth dynamics', in *ASME International Mechanical Engineering Congress and Exposition*, Dallas, TX, 1997.
25. Slavič, J. and Boltežar, M., 'Nonlinearity and non-smoothness in multi body dynamics: Application to woodpecker toy', *Journal of Mechanical Engineering Science*, in press, 2005.
26. Stewart, D., 'Rigid-body dynamics with friction and impact', *SIAM Review* **42**(1), 2000, 3–39.
27. Stewart, D. and Trinkle, J., 'An implicit time-stepping scheme for rigid body dynamics with inelastic collisions and coulomb friction', *Journal of Numerical Methods Engineering* **39**, 1996, 2673–2691.
28. Tabor, D., 'Friction-The present state of our understanding', *Journal of Lubrication Technology* (183), 1981, 169–179.
29. Vereshchagin, A., 'Computer simulation of the dynamics of complicated mechanisms of robot manipulations', *Engineering Cybernetics* **6**, 1974, 65–70.
30. Wösle, M. and Pfeiffer, F., 'Dynamics of spatial structure-varying rigid multibody systems', *Archive of Applied Mechanics* **69**(4), 1991, 265–285.
31. Zhao, X., Reddy, C., and Nayfeh, A., 'Nonlinear dynamics of an electrically driven impact microactuator', *Nonlinear Dynamics* **40**(3), 2005, 227–239.